

Chapter 79

Analytical Modelling of Integrated Solar Drying System

M. A. Karim and Zakaria Mohd. Amin

Abstract The drying of fruit and vegetables is a subject of great importance. Dried fruit and vegetables have gained commercial importance, and their growth on a commercial scale has become an important sector of the agricultural industry. However, food drying is one of the most energy intensive processes of the major industrial process and accounts for up to 15% of all industrial energy usage. Due to increasingly high electricity prices and environmental concern, a dryer using traditional energy sources is not a feasible option anymore. Therefore, an alternative/renewable energy source is needed. In this regard, an integrated solar drying system that includes highly efficient double-pass counter flow v-groove solar collector, conical-shaped rock-bed thermal storage, auxiliary heater, the centrifugal fan and the drying chamber has been designed and constructed. Mathematical model for all the individual components as well as an integrated model combining all components of the drying system has been developed. Mathematical equations were solved using MATLAB program. This paper presents the analytical model and key finding of the simulation.

Keywords Solar drying · V-groove collator · Rock-bed thermal storage · Conical tank

Nomenclature

D_h, D'_h	Hydraulic diameter of first and second pass (m)
$h_{1,2,3,4}$	Convection heat transfer coefficients (W/m^2K)
h_{rs}	Glass cover to sky radiative heat transfer coefficient (W/m^2K)
$h_{r21,r23}$	Radiative heat transfer coefficient (W/m^2K)
h_w	Wind convection heat transfer coefficient (W/m^2K)
H_c	Gap between v-groove absorber and glass cover (m)
H_g	Height of v-groove (m)
I	Solar radiation (W/m^2)
k	Thermal conductivity of air (W/mk)

M. A. Karim (✉) · Z. M. Amin
Mechanical Engineering Discipline, Science and Engineering Faculty,
Queensland University of Technology, Brisbane, Australia
e-mail: azharul.karim@qut.edu.au

© Springer International Publishing Switzerland 2016
A. Sayigh (ed.), *Renewable Energy in the Service of Mankind Vol II*,
DOI 10.1007/978-3-319-18215-5_79

k_i	Insulation thermal conductivity (W/mk)
L	Length of the collector (m)
m	Air mass flow rate ($\text{kg/m}^2\text{s}$)
n_c	Efficiency of the collector
N	Number of glass cover
$Q_{1,2}$	Heat transferred to the air in first and second pass (W/m^2)
$S_{1,2}$	Solar radiation absorbed by glass cover and absorber plate (W/m^2)
$T_{1,2,3,4}$	Mean temperatures of surfaces (K)
T_a	Ambient temperature (K)
$T_{f1,f2}$	Mean fluid temperature (K)
T_s	Sky temperature (K)
T_{fi}	Initial air temperature (K)
T_o	Output air temperature (K)
U_b	Bottom heat loss coefficient ($\text{W/m}^2\text{K}$)
U_t	Top heat loss coefficient ($\text{W/m}^2\text{K}$)
U_f	Air velocity in the collector (m/s)
V	Wind velocity (m/s)
W	Width of the collector (m)
x	Insulation thickness (m)
α_1	Absorptivity of glass cover
ε_1	Emissivity of glass cover
τ_1	Transmittance of glass cover
σ	Boltzmann constant ($5.67 \times 10^{-8} \text{W/m}^2\text{K}^4$)
ρ	Air density (kg/m^3)
\varnothing	Tilt angle of the collector (degrees)
μ	Dynamic viscosity (kg/ms)
A	Area (m)
h_v	Volumetric heat loss coefficient ($\text{W/m}^3 \text{ }^\circ\text{C}$)
L	Length (m)
\dot{m}	Mass flow rate (kg/ms)
N	Number of bed elements
T_{amb}	Ambient air temperature ($^\circ\text{C}$)
$T_{a,m}$	Inlet air temperature to bed element ($^\circ\text{C}$)
$T_{b,m}$	Mean temperature of bed element ($^\circ\text{C}$)
$T_{a,m+1}$	Outlet air temperature of bed element ($^\circ\text{C}$)

79.1 Introduction

Traditional sun drying is a labour-extensive, time-consuming slow process with requirement of large area [1]. Also, quality of the product cannot be maintained as there is no control on the drying process. On the other hand, the use of mechanical drying using fossil fuel or electricity will solve quality problem that occurs during

traditional sun drying but is highly energy intensive and expensive. Furthermore, most small farmers cannot afford this technology and cost of fossil fuel [2]. These drawbacks can be solved by the use of solar dryer. However, initial cost of solar dryers can be considered high and therefore payback period should be low to make this technology attractive. To make the payback period shorter, the solar dryer needs to be very efficient [3].

To successfully develop an efficient solar drying system, it is important to design an air collector with high efficiency since it is one of the main components and would lead to a better performance of the system [4]. Flat plate air collectors are widely used; however, out of the three collector plates (namely flat plate, v-corrugated and finned air collectors) studied in [5], v-corrugated collector has higher efficiency, thus considered to be better for the solar drying system. The efficiency is further increased in double-pass operation, and optimal flow rate is determined to be $0.035 \text{ kg/m}^2 \text{ s}$ [5]. A mathematical model was also developed and compared the results with the experiments [6]. Systems using solar energy only operate during hours of adequate sunlight; therefore, to increase the reliability of the system, thermal storages need to be used. Thermal energy stored may be used later when solar energy is not available or sufficient. The packed bed storage system consisting of loosely packed rock material is considered most suitable for solar drying [7]. Literature shows that conical-shaped thermal storage tank is suitable for small-scale operation.

In this research, an integrated solar drying system is designed and constructed. Mathematical models for the major component and the entire system were developed. The models were solved using MATLAB program.

79.2 Solar Drying System

The principal components of solar drying systems are solar air collector which is used for heating ambient air, a drying unit where air extracts moisture from the product and the air handling unit which circulates the air. A thermal storage tank can be added to store energy for later use, as in Fig. 79.1.

As mentioned above, the solar air collector being investigated is a double-pass counter flow v-groove air collector in which the inlet air initially flows at the top part of the collector and changes direction once it reaches the end of the collector and flows below the collector to the outlet. As shown in Fig. 79.1, the outlet air from the solar collector then goes to the branched section in which the air flow is divided. The amount of air flow in each branch depends on the current setting of the valves and condition of the air. For example, if the output air temperature of the solar collector exceeds the current requirement at the drying chamber, higher percentage of the air will go through the thermal storage tank. Where there is no drying, all the air will go to the thermal storage. Control of air flow leads to a more flexible system, which can operate at optimum conditions. At times of low sunlight or when it is night-time, the stored energy in the thermal storage will be discharged, thus allow-

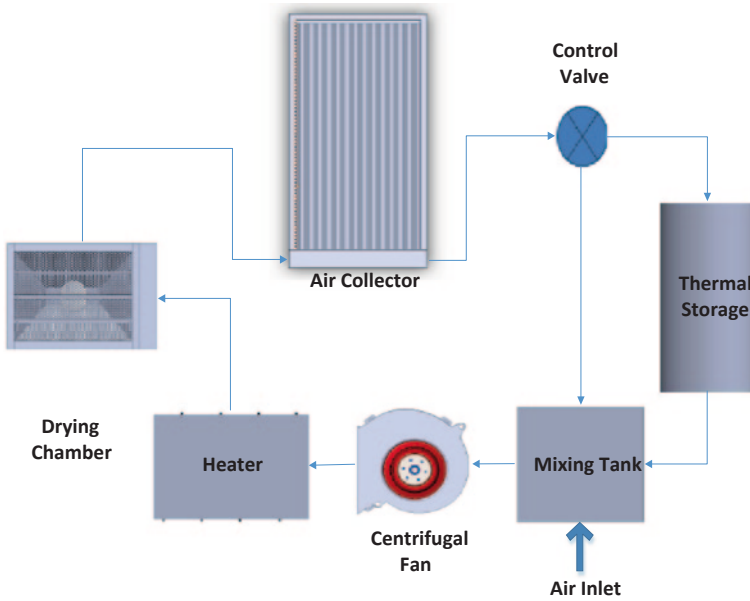


Fig. 79.1 Solar drying system components

ing the hot air to be used for drying. The auxiliary heater at the inlet of the drying chamber is used for back up heating or for maintaining a constant air temperature at the inlet of the drying chamber.

79.3 Mathematical Modelling

79.3.1 Solar Air Collector

A readily available analytic model for the double-pass counter flow v-groove solar air collector is not found in the literature. Thus, to investigate the solar collector performance and calculate its operating parameters such as temperature, development of the model from basic heat balance equations is necessary. The solution involves iterative matrix method to calculate output parameters. Figure 79.2 shows the collector cross section and thermal network of the double-pass V-groove collector.

Energy balance equations based on the thermal network shown in Fig. 79.2 for the glass cover, first-pass fluid, absorber plate, second-pass fluid and back plate are given in the equations below.

The energy balance in the top plate is given by

$$S_1 + h_{r21}(T_2 - T_1) + h_1(T_{f1} - T_1) = U_T(T_1 - T_a)$$

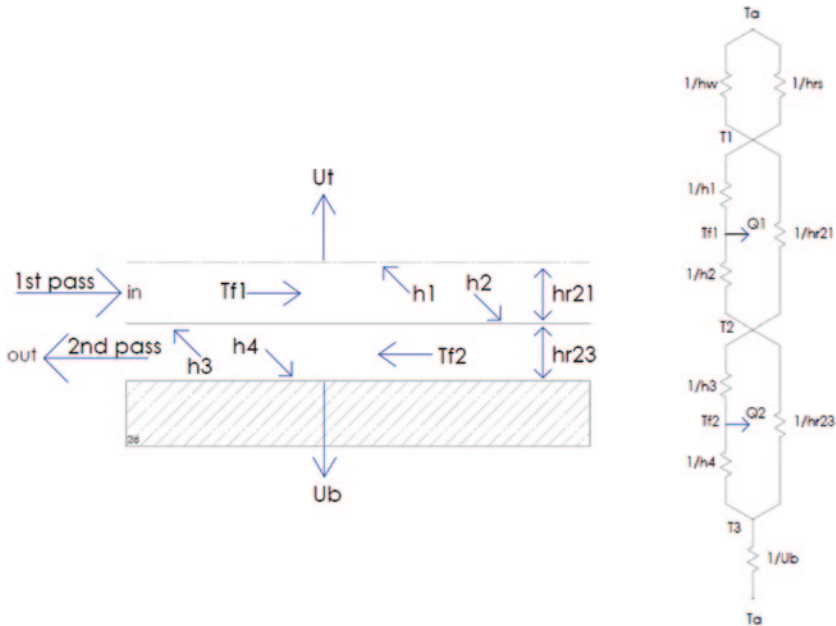


Fig. 79.2 Cross section and thermal network of a double-pass v-groove solar air collector

For the fluid's first pass,

$$h_2(T_2 - T_{f1}) = h_1(T_{f1} - T_1) + Q_1$$

Energy balance in the absorber plate is

$$S_2 = h_3(T_2 - T_{f2}) + h_2(T_2 - T_{f1}) + h_{r23}(T_2 - T_3) + h_{r21}(T_2 - T_1)$$

For the fluid's second pass,

$$h_3(T_2 - T_{f2}) = h_4(T_{f2} - T_3) + Q_2$$

For the bottom plate,

$$h_4(T_{f2} - T_3) + h_{r23}(T_2 - T_3) = U_b(T_3 - T_a)$$

These equations are then arranged in terms of temperature and placed in a 5×5 matrix in the form of

$$[A][T] = [B]$$

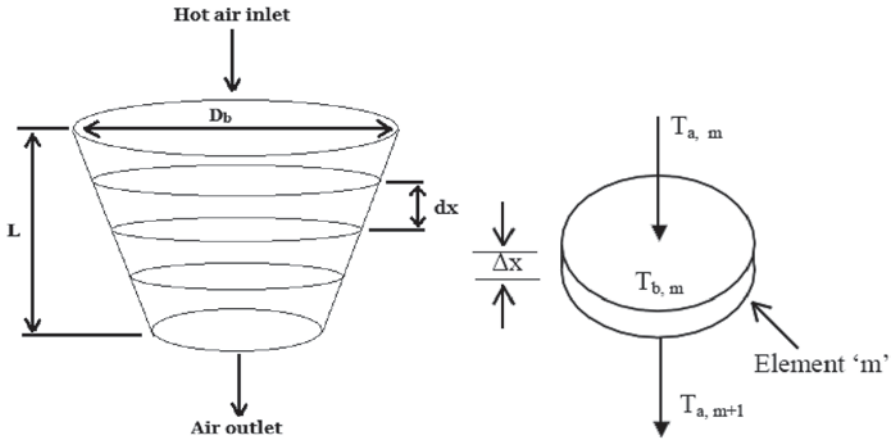


Fig. 79.3 Conical thermal storage tank (left) and element 'm' of the tank (right)

The mean temperature can be determined by using array division

$$[T] = [A]^{-1}[B]$$

79.3.2 Thermal Storage Tank

To model the storage tank mathematically, the length (height) L of the storage tank is divided into several nodal elements dx as depicted in Fig. 79.3. The value of dx is small and only exaggerated in the figure.

The following governing temperatures are used to evaluate the temperature distribution for air and solid in the thermal storage tank

$$T_{a,m+1} = T_{b,m} + (T_{a,m} - T_{b,m}) \exp(-\phi_1)$$

$$\phi_1 = \frac{h_v AL}{N(\dot{m}_a C p_a)} = \frac{NTU}{N}; \quad N = \frac{L}{\Delta x}$$

$$T_{b,m(t+\Delta t)} = T_{b,m(t)} + \left[\phi_2 (T_{a,m} - T_{a,m+1}) - \phi_3 (T_{b,m} - T_{amb}) \right] \Delta t$$

$$\phi_2 = \frac{\dot{m}_a C p_a N}{(\rho_r C p_r) AL (1 - \epsilon)}; \quad \phi_3 = \phi_2 \left(\frac{U \Delta A_m}{\dot{m}_a C p_a} \right)$$

Neglecting loss to the surroundings, $T_{b,m(t+\Delta t)}$ becomes

$$T_{b,m(t+\Delta t)} = T_{b,m(t)} + \left[\phi_2 (T_{a,m} - T_{a,m+1}) \right] \Delta t$$

79.3.3 Auxiliary Heater

Air flows through the heater with a known mass flow rate and inlet temperature. Assuming a constant heat transfer and negligible heat loss to the environment, the performance of the auxiliary heater is determined by the simple equation

$$\dot{Q} = \dot{m}C_p[T_2 - T_1]$$

79.3.4 Drying Chamber

79.3.4.1 Material Model

The moisture balance equation is $\frac{\partial M}{\partial t} + u \frac{\partial M}{\partial x} = D_{\text{eff}} \frac{\partial^2 M}{\partial x^2}$

Temperature balance equation is $\frac{\partial T}{\partial t} + u \frac{\partial T}{\partial x} = D_{\text{eff}} \frac{\partial^2 T}{\partial x^2}$

With initial condition at $t=0$, $M = M_0$ and $T = T_0$

Boundary condition at $x=0$, $\frac{\partial M}{\partial t} = 0$ and $\frac{\partial T}{\partial t} = 0$

Effective diffusivity is $\frac{D_{\text{ref}}}{D_{\text{eff}}} = \left(\frac{b_0}{b}\right)^2$

Thickness ratio is obtained by the following equation

$$b = b_0 \left[\frac{\rho_w + M_w \rho_s}{\rho_w + M_0 \rho_s} \right]$$

79.3.4.2 Equipment Model

The energy balance at the drying chamber is

$$\frac{\partial T_a}{\partial z} = \frac{\rho_s (C_s + C_m M)(1 - \epsilon)}{(G_0 C_{pa})} \frac{\partial T}{\partial t} + \frac{\partial M}{\partial t} h_{fg} \frac{\rho_s (1 - \epsilon)}{G_0 C_{pa}}$$

The moisture balance is

$$\frac{\partial Y}{\partial z} = \frac{\rho_s (1 - t)}{G_0} \frac{\partial M}{\partial t}$$

Boundary and initial conditions are as follows:

At $x=0$ and $t=0$,

$$T_a = T_0 \text{ and } Y = Y_0$$

$$\frac{dT_a}{dt} = 0 \text{ and } \frac{dY}{dt} = 0.$$

At $x>0$ and $t=0$,

$$T_a = T_0 \text{ and } Y = Y_0$$

The differential equations are discretized and written in finite difference form before performing simulation.

79.4 Results and Discussion

The entire solar drying system is simulated in MATLAB. The initial key parameters are presented in Table 79.1.

The figures below show how the temperature changes as it progresses through each component. In Fig. 79.4, the output air temperature in the double-pass v-groove air collector is plotted against time. It also shows the temperature of the input air. It can be seen from the graph the change in temperature of the air once it passed through the air collector. The maximum output temperature occurs at 1:00 pm, which is approximately 315 K.

In the exit of the solar air collector, there is a branch. For the current simulation, 100% air passed through the storage tank. From Fig. 79.5, it can be seen that in the first few hours, the output air temperature of the thermal storage is very low as energy is used to heat the rocks and energy is stored in the rocks. Then, as time progress, the output air temperature in the thermal storage increases. It is interesting to see that, around 5 pm, when the solar radiation is quite low, output temperature from the storage is still quite high and the thermal storage tank is charged during the day. In Fig. 79.6, it can be seen that the input temperature from storage overlaps the output temperature. This is because in the current operation, all the air flows to the thermal storage and no air flow from the collector goes to the mixing tank. If the proportion is changed, then the output temperature will be somewhere in between the two air temperatures from the collector and storage tank. In Fig. 79.7, the auxiliary heater increased the air temperature before it goes to the drying chamber.

Then, in Fig. 79.8, the temperature change through the system is shown. It can be seen that the air temperature increases by approximately 40 °C, which is a desirable result. The temperature range of the air going to the drying chamber is ideal for drying apple as determined by [8]; thus, for the simulation study, the air temperature

Table 79.1 Variables considered in drying tests.

Mass flow rate (kg/s)	0.1
Drying duration (h)	7
Sample (apple) weight (kg)	1.72
Number of samples (apple)	45
Sample thickness (mm)	10
Heater size (kW)	3
Air velocity (m/s)	0.61

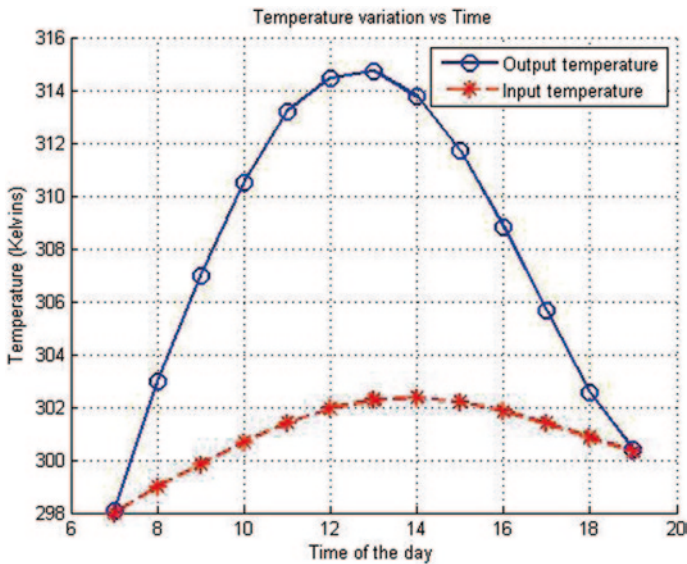


Fig. 79.4 Solar air collector inlet and outlet air temperature

entering the drying chamber may be 60–80°C for faster drying time and better quality product.

The hot air coming out from the heater goes to drying chamber, as represented in the set-up schematic in Fig. 79.1. The drying curves of the material (apple) are presented in Figs. 79.9 and 79.10. For both the figures, initial rate of moisture removal and rate of temperature rise are high. It can also be seen that both moisture removal rate and temperature rise stabilize after 2 pm. Thus, these curves follow the normal drying trend of apple [8].

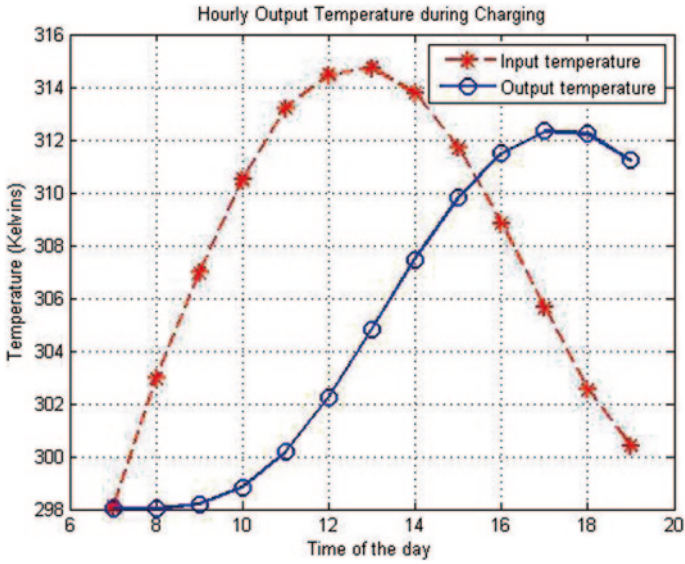


Fig. 79.5 Rock-bed storage tank inlet and outlet temperature

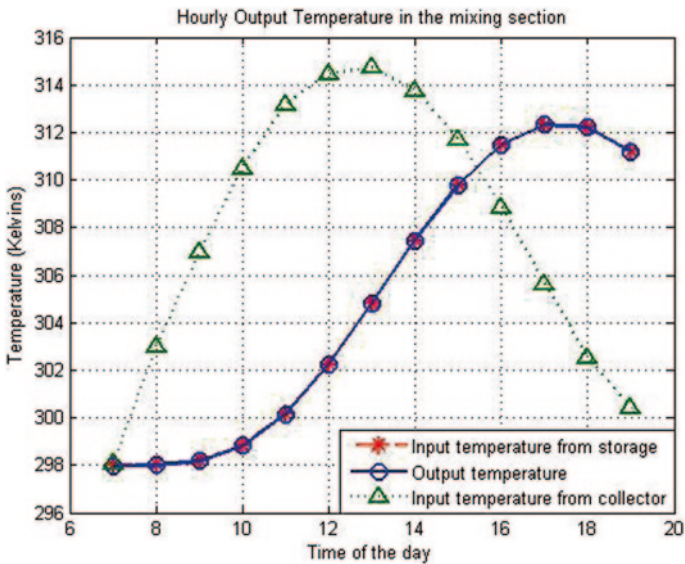


Fig. 79.6 Outlet temperature from mixing chamber

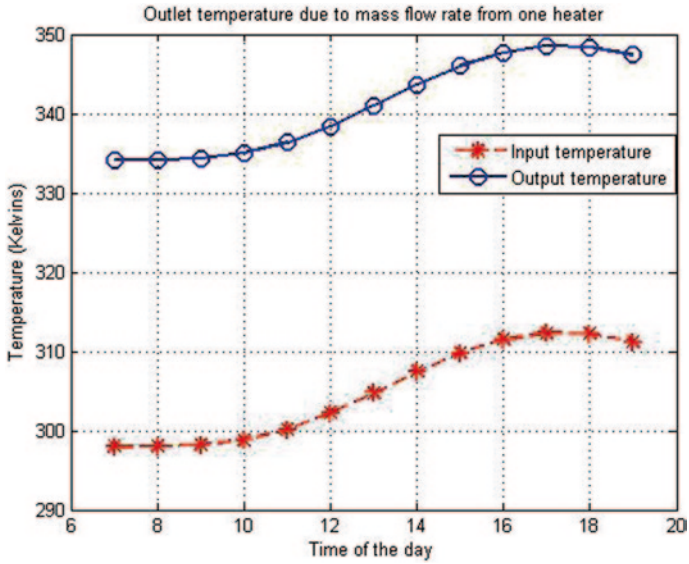


Fig. 79.7 Output temperature from the auxiliary heater

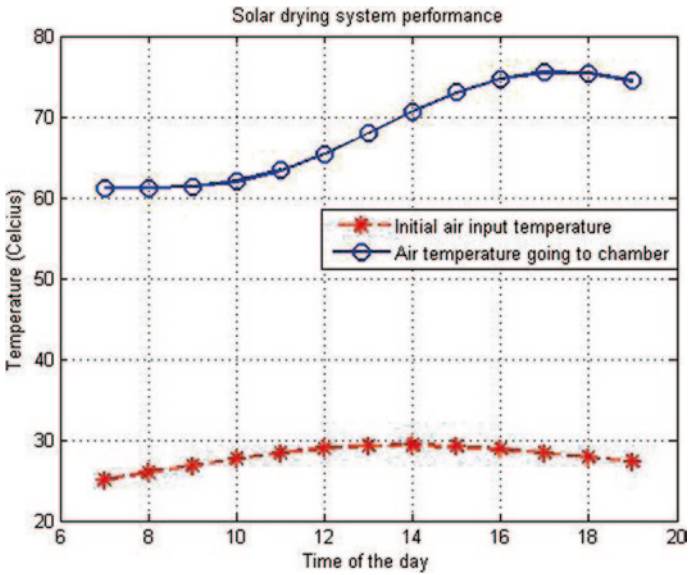


Fig. 79.8 Total increase in temperature of the solar drying system

Fig. 79.9 Drying moisture curve

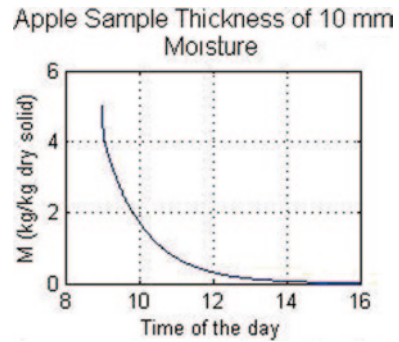
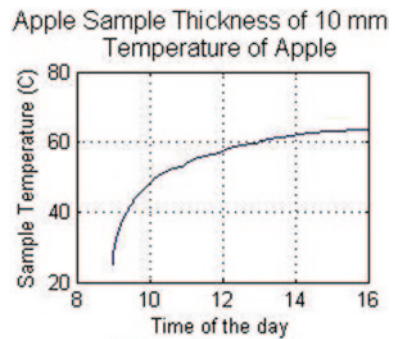


Fig. 79.10 Drying material temperature curve



79.5 Conclusion

The mathematical model was able to predict the mean temperature, the instantaneous air temperature, the output air temperature and efficiency of any component of the drying system. The thermal performance of the thermal storage tank, drying chamber and heater was determined using the mathematical model developed, which were then interconnected by MATLAB codes to simulate the whole system. The parameters determined by the model are considered very important to design any drying system for specific drying purposes. Present study provided the much needed integrated model which is absent in the literature. The temperature range in which the system will run is between 60 and 80 °C. This is the ideal drying temperature for apple. Along with an air velocity entering the drying chamber at 1–2 m/s and air humidity as low as possible, the drying time can be greatly reduced and the product quality is improved.

References

1. Shalaby SM, El-Sebaai AA (2012) Solar drying of agricultural products: a review. *Renew Sustain Energy Rev* 16:37–43
2. Chua KJ, Mujumdar AS, Hawlader MNA, Chou SK, Ho JC (2001) Convective drying of agricultural products. Effect of continuous and stepwise change in drying air temperature. *Dry Technol* 19(8):1949–1960
3. VijayaVenkataRaman S, Iniyan S (2012) A review of solar drying technologies. *Renew Sustain Energy Rev* 16:2652–2670
4. Karim MA, Hawlader MNA (2006) Performance investigation of flat plate, v-corrugated and finned air collectors. *Energy* 31:452–470
5. Karim MA, Hawlader MNA (2006) Performance evaluation of v-groove solar air collector for drying applications. *Appl Therm Eng* 26:121–130
6. Karim MA, Perez E, Amin ZM (2014) Mathematical modelling of counter flow v-groove solar air collector. *Renew Energy J* 67:192–201
7. Karim MA, Amin ZM (2014) Mathematical modelling of rock-bed solar thermal storage tank. Solar 2014 Conference, Melbourne, Australia, May-2014
8. Menges HO, Ertekin C (2006) Mathematical modeling of thin layer drying of Golden apples. *J Food Eng* 77:119–125